

# Achiral Bent-Core Liquid Crystals with Azo and Azoxy Linkages: Structural and Nonlinear Optical Properties and Photoisomerization

C. L. Folcia,<sup>†</sup> I. Alonso,<sup>†</sup> J. Ortega,<sup>\*,‡</sup> J. Etxebarria,<sup>†</sup> I. Pintre,<sup>§</sup> and M. B. Ros<sup>§</sup>

*Departamento de Física de la Materia Condensada, Facultad de Ciencia y Tecnología, Universidad del País Vasco, 48080 Bilbao, Spain, Departamento de Física Aplicada II, Facultad de Ciencia y Tecnología, Universidad del País Vasco, 48080 Bilbao, Spain, and Instituto de Ciencia de Materiales de Aragón, Química Orgánica, Facultad de Ciencias, Universidad de Zaragoza-CSIC, 50009 Zaragoza, Spain*

Received February 2, 2006. Revised Manuscript Received June 29, 2006

We present a structural study of the mesophases of three achiral bent-core compounds with azo and azoxy bonds. The study is based on textures observation and small-angle X-ray diffraction. It is found that the materials exhibit columnar and tilted smectic mesophases. Optical second-harmonic generation measurements are performed on aligned samples of one of the compounds, and the whole second-order susceptibility tensor is determined. Finally, some simple aspects of the photoisomerization of the materials are examined.

## Introduction

In the past few years, the discovery of achiral bent-core mesogens (also known as banana-shaped liquid crystals) has given rise to an increase of the research activity in the field of ferroelectric liquid crystals.<sup>1–4</sup> This growth in interest is due essentially to the peculiar properties of these new materials regarding the chirality and polarity. It has also been pointed out that these compounds have some potentialities for applications in the field of nonlinear optics.<sup>5–7</sup> Most of these studies have been carried out in the  $B_2$  (SmCP) phase, which usually displays antiferroelectric switching. In contrast, other mesophases such as the  $B_7$  phase have been much less studied. Even the name of the phase itself is object of some controversy. In principle, the designation  $B_7$  responds to a special type of optical textures under the polarizing microscope.<sup>8</sup> The structure of the phase responsible of the textures is not totally clarified, and it even seems that different structures are classified under the same name.<sup>4,9–11</sup> The information about this point is scarce, and in this sense, it seems of interest to perform new structural studies on this phase.

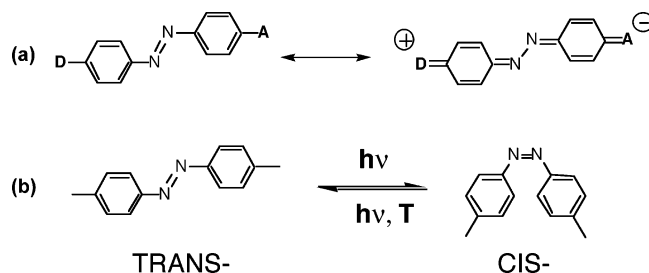


**Figure 1.** Simple models to explain the optical responses of the bent-core molecules considered in this work. (a) The optical nonlinearities of the lateral cores of the molecule are schematized in terms of a delocalized electronic charge distribution between donor (D) and acceptor (A) groups at both sides of the  $\pi$  system of an azo (or azoxy) -benzene structure. (b) The azo (or azoxy) bonds undergo isomerization cycles between the trans and the cis states by illumination.

It is well-known in the liquid-crystal field that the chemical structure is one of the key points that determines the supramolecular packing and, hence, the properties of the mesomorphic material. Thus, a proper molecular design could allow achieving not only an aimed mesophase but also a multifunctional material. In this work we will explore new bent-core structures containing azo or azoxy linkages. The interest of the azobenzene or azoxybenzene structures is based on two reasons. One is that these systems allow delocalized electronic charge distribution between donor and acceptor groups at both sides of the  $\pi$  system, as schematized in Figure 1a. This possibility is interesting for the design of materials with good nonlinear optical properties. In particular for optical second-harmonic generation (SHG), the azo and

\* Corresponding author. E-mail: josu.ortega@ehu.es.  
<sup>†</sup> Departamento de Física de la Materia Condensada, Universidad del País Vasco.

<sup>‡</sup> Departamento de Física Aplicada II, Universidad del País Vasco.

<sup>§</sup> Universidad de Zaragoza-CSIC.

- (1) Niori, T.; Sekine, T.; Watanabe, J.; Furukawa, T.; Takezoe, H. *J. Mater. Chem.* **1996**, *6*, 1231.
- (2) Pelzl, G.; Diele, S.; Weissflog, W. *Adv. Mater.* **1999**, *11*, 707.
- (3) Link, D. R.; Natale, G.; Shao, R.; MacLennan, J. E.; Clark, N. A.; Körblova, E.; Walba, D. M. *Science* **1997**, *278*, 1924.
- (4) Amaranatha Reddy R.; Tschierske, C. *J. Mater. Chem.* **2006**, *16*, 907.
- (5) Macdonald, R.; Kentischer, F.; Warnick, P.; Heppke, G. *Phys. Rev. Lett.* **1998**, *81*, 4408.
- (6) Araoka, F.; Thisayukta, J.; Ishikawa, K.; Watanabe, J.; Takezoe, H. *Phys. Rev. E* **2002**, *66*, 021705.
- (7) (a) Ortega, J.; Gallastegui, J. A.; Folcia, C. L.; Etxebarria, J.; Gimeno, N.; Ros, M. B. *Liq. Cryst.* **2004**, *31*, 579. (b) Gallastegui, J. A.; Folcia, C. L.; Etxebarria, J.; Ortega, J.; Gimeno, N.; Ros, M. B. *J. Appl. Phys.* **2005**, *98*, 83501.
- (8) Pelzl, G.; Diele, S.; Jakli, A.; Lischka, Ch.; Wirth, I.; Weissflog, W. *Liq. Cryst.* **1999**, *26*, 135.

- (9) Coleman, D. A.; Fernsler, J.; Chattham, N.; Nakata, M.; Takamishi, Y.; Körblova, E.; Link, D. R.; Shao, R. F.; Jang, W. G.; MacLennan, J. E.; Mondainn-Mova, O.; Boyer, C.; Weissflog, W.; Pelzl, G.; Chien, L. C.; Zasadzinski, J.; Watanabe, J.; Walba, D. M.; Takezoe, H.; Clark, N. A. *Science* **2003**, *301*, 1204.
- (10) Pelzl, G.; Schröder, M. W.; Dunemann, U.; Diele, S.; Weissflog, W.; Jones, C.; Coleman, D.; Clark, N. A.; Stannarius, R.; Li, J.; Das B.; Grande, S. *J. Mater. Chem.* **2004**, *14*, 2492.
- (11) Folcia, C. L.; Etxebarria, J.; Ortega, J.; Ros, M. B. *Phys. Rev. E* **2005**, *72*, 041709.

azoxybenzene structures seem to be good candidates to be incorporated in the lateral cores of the bent-shaped molecules.

An additional attractive feature of the azo and the azoxy groups is the transformation between their trans and cis configurations by light absorption (photoisomerism;<sup>12</sup> Figure 1b). In the field of liquid crystals this property gives rise to a new added value to the materials, which can be used for photoalignment.<sup>13</sup> In this respect not much work has been published with bent-core mesogens, though some photoinduced effects in a few electric or optical properties have been observed.<sup>14–18</sup>

In this work we present a characterization study of three bent-core liquid crystals with azo- and azoxybenzene structures. Basically it is a structural study based on textures observation and small-angle X-ray scattering. In addition, we have also carried out SHG measurements on monodomain samples and have characterized the whole tensor for the second-order nonlinear susceptibility in one of the materials. Finally we analyze qualitatively some simple aspects of the photoisomerism within the mesophases.

### Experimental Section

The chemical structures and phase sequences of the studied materials are shown in Figure 2. The synthetic procedures for the different bent-core compounds are shown in Scheme 1. In all cases, synthetic methods reported in the literature for the same compounds or adapted to the aimed ones have been followed. Experimental details as well as their structural characterization have been included as Supporting Information.

The phase assignment will be discussed below. As can be seen, compounds C1 and C2 have one azo or one azoxy group in both lateral structures of the molecule, respectively. Compound C3 presents only one azo group. In the three cases the photoactive bond connects a donor (the alkyloxy terminal tail) and an acceptor moiety (carboxyl group) both, in the para position of the  $\pi$  system.

For the electrooptic study, samples were prepared in commercially available cells (Linkam) of nominal thickness of 5  $\mu\text{m}$ . X-ray measurements on nonoriented samples were performed using a small-angle goniometer equipped with a high-temperature attachment, a linear position-sensitive detector of 4° of angular range, and an angular resolution better than 0.01°. Monochromatic Cu K $\alpha$  radiation was used. The materials were introduced in the isotropic phase into Lindemann capillaries of diameter 0.5 mm. SHG measurements were carried out in homemade cells with in-plane electrodes, using gaps of 100  $\mu\text{m}$ . We employed glass spheres as spacers, and the resulting thicknesses were about 10  $\mu\text{m}$ . The measurements were performed with a standard experimental setup described elsewhere.<sup>19</sup> The fundamental light is a Q-switched Nd:YAG laser (wavelength 1064 nm) with a pulse width of 6 ns and

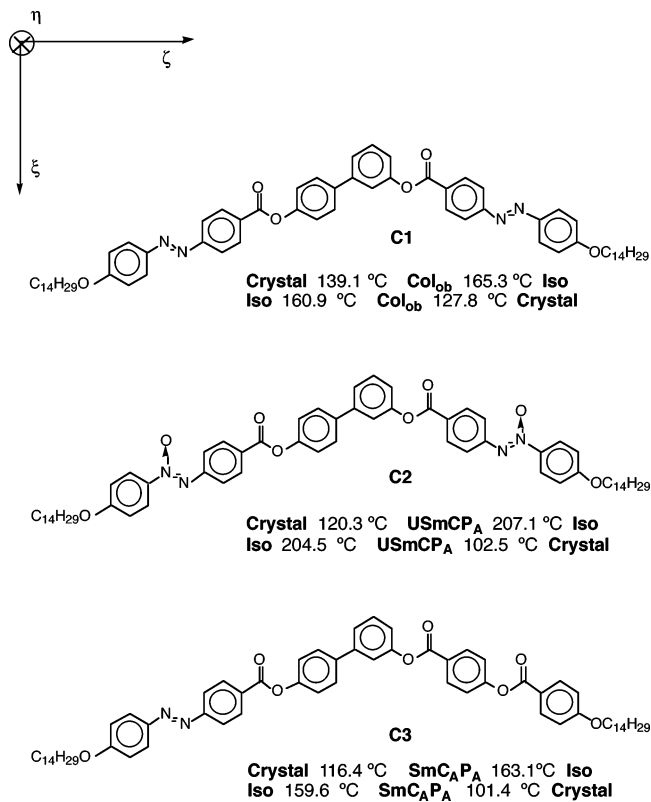


**Figure 2.** Chemical structures and phase sequences on heating and cooling of the studied materials. In the figure Col<sub>ob</sub> makes reference to a columnar oblique phase, USmCP<sub>A</sub> indicates an undulated smectic C antiferroelectric polar phase, and SmC<sub>A</sub>P<sub>A</sub> corresponds to an anticlinic smectic C phase with antiferroelectric polar order.

a frequency of 5 Hz. A square-wave electric field synchronized to the laser pulse was applied to the sample, and it was always checked that the field was strong enough for the saturation of the SHG signal.

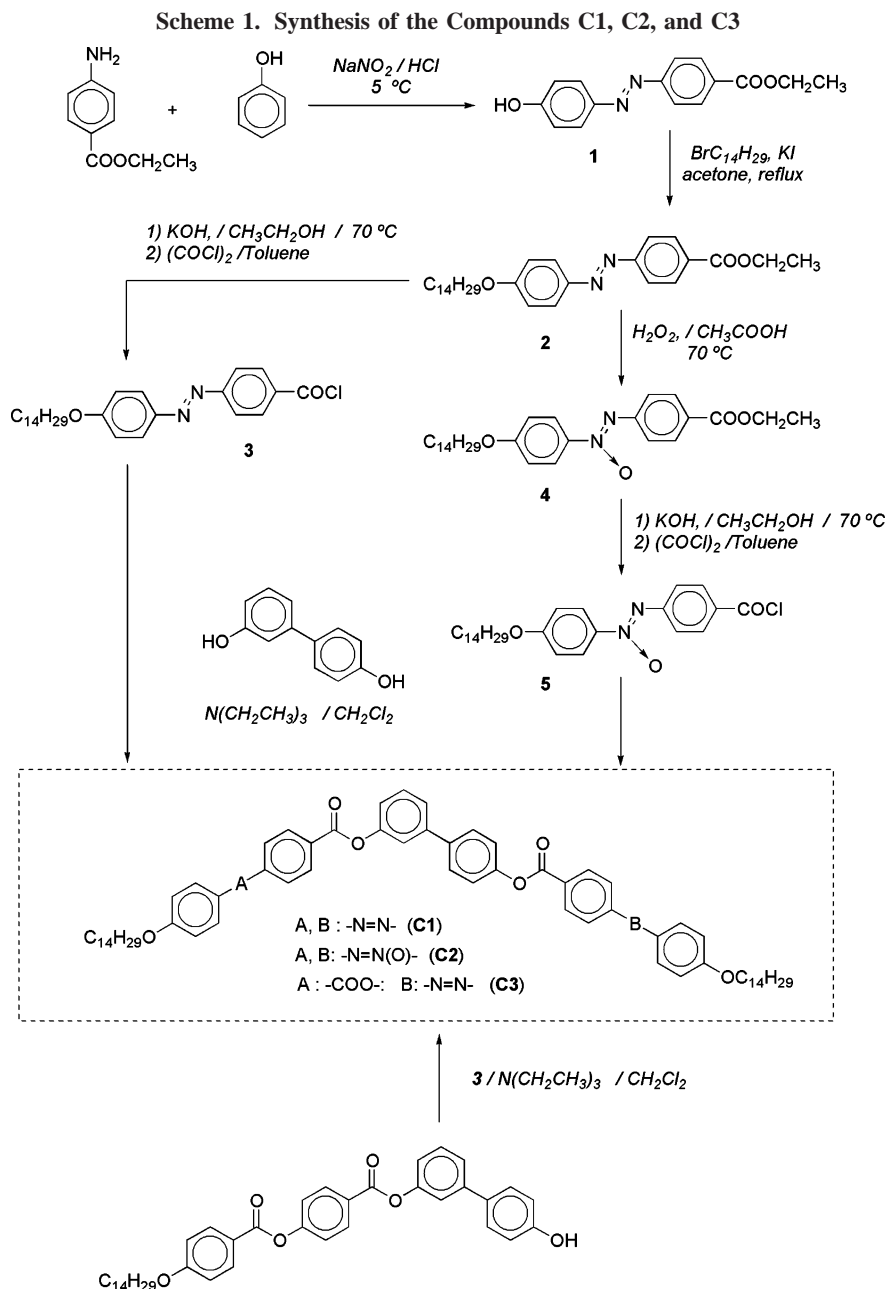
### Results Obtained for the Material C1

A first characterization of the liquid crystal phase of compound C1 was performed through the analysis of the optical textures and electrooptic behavior. Figure 3a shows the texture observed between crossed polarizers when the sample was cooled from the isotropic phase. The general aspect is characteristic of a columnar ( $B_1$  type) phase: long-shaped domains (banana leaves), which are pinkish colored in this case, together with broken focal conics and small fan-shaped domains. The stability of this phase ranges from 139 °C to 165 °C. On the other hand, the material displays a relatively high birefringence (a value of  $\Delta n = 0.36$  was measured at the banana leaves and other oriented domains), suggesting either a nontilted or a synclinc structure, where the molecular dipoles are perpendicular to the glass plates. Such high values for  $\Delta n$  are normal in materials based on azo molecules.<sup>13</sup>

Further information concerning the molecular orientation at the banana leaves can be deduced from Figure 3. It can be seen that the upper and lower halves of the leaves in Figure 3a have the same color and show almost simultaneous extinction when the central defect line makes 45° with respect

- (12) (a) Eich, M.; Wendorff, J. H.; Beck, B.; Ringsdorf, H. *Makromol. Chem., Rapid Commun.* **1987**, *8*, 59. (b) Sie, S.; Natasohn, A.; Rochon, P. *Chem. Mater.* **1993**, *5*, 403. (c) Natasohn, A.; Rochon, P. *Chem. Rev.* **2002**, *102*, 4139. (d) Chanishvili, A.; Chilaya, G.; Petriashvili, G.; Collings, P. J. *Phys. Rev. E* **2005**, *71*, 051705.
- (13) Hagen, R.; Bieringer, T. *Adv. Mater.* **2001**, *13*, 1805.
- (14) Nair, G. G.; Prasad, S. K.; Hiremath U. S.; Yelamaggad, C. V. *J. Appl. Phys.* **2001**, *90*, 48.
- (15) Kim, H.; Lim, T. K.; Shin, S. T.; Lee, C. K.; Araoka, F.; Ofuji, M.; Takamishi, Y.; Takezoe, H. *Phys. Rev. E* **2004**, *69*, 061701.
- (16) Prasad, V.; Kang, S. W.; Qi, X.; Kumar, S. *J. Mater. Chem.* **2005**, *14*, 1495.
- (17) Prasad V.; Jakli, A. *Liq. Cryst.* **2004**, *31*, 473.
- (18) Jakli, A.; Prasad, V.; Rao, D. S. S.; Liao, G.; Janossy, I. *Phys. Rev. E* **2005**, *71*, 021709.

- (19) Pereda, N.; Folcia, C. L.; Etxebarria, J.; Ortega, J.; Ros, M. B. *Liq. Cryst.* **1998**, *24*, 451.



to the polarizing directions (see Figure 3b). On the other hand, the rapid and slow axes were identified at both halves of a given leaf with a Berek compensator. We found that the optical indicatrix on one half is rotated  $90^\circ$  with respect to the one of the other half. There is a unique conclusion compatible with these observations: the molecular directors on both halves of the leaves make an angle of  $45^\circ$  with respect to the defect line at the center of the leaf.

Next, a low frequency electric field was applied perpendicularly to the glass plates to study the electrooptic behavior of this material. No change was detected for weak fields. However, when the field was higher than a threshold value of about  $10 \text{ V}/\mu\text{m}$ , the texture broke down into very small domains and showed a nondefined response to the field variation. Therefore, it seems that a phase transition was induced by the electric field, but no characterization of the new phase was possible from simple texture observation. When the sample was cooled from the isotropic phase under

the electric field, a different texture was obtained (see Figure 4a) with large focal conic domains, characteristic of a smectic phase. The extinction brushes made an angle of about  $45^\circ$  with respect to the polarizing directions, and the material switched between both ferroelectric states with the field polarity (clockwise and counterclockwise rotations of the extinction brushes occurred under low-frequency triangular voltage). This behavior indicates unambiguously that the structure under field is synclitic with a tilt close to  $45^\circ$ . It can, therefore, be concluded that, in the present conditions, the mesophase is homogeneously chiral smectic (SmCP type). Accordingly, Figure 4b shows the texture observed when the electric field is removed. The extinction brushes are now parallel to the polarizing directions (the structure is anticlinic), and the gray color is due to the nearly orthoconic situation corresponding to a  $\text{SmC}_A\text{P}_A$  structure with a tilt angle close to  $45^\circ$ , which provokes an important decrease of the birefringence. In summary, taking into account the

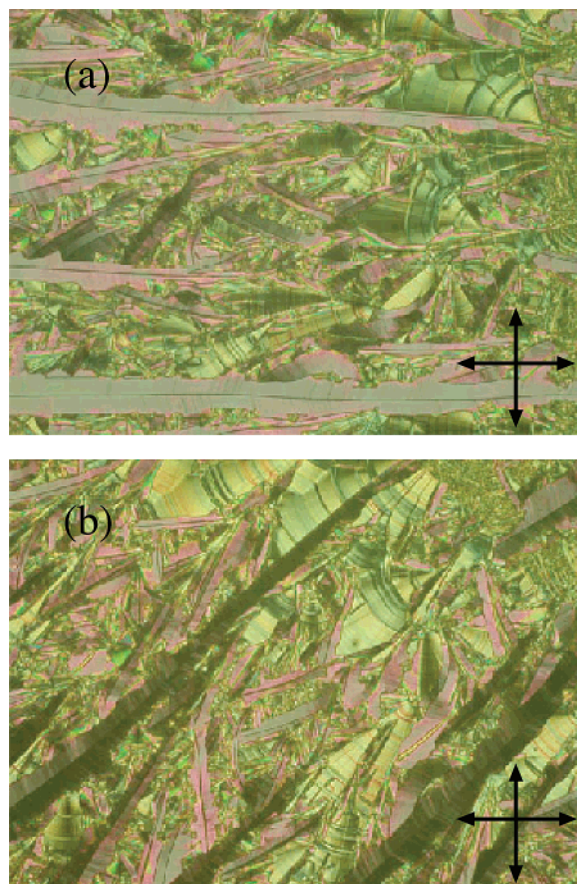


**Figure 3.** Photomicrographs of the textures of compound C1 in the Colob phase. (a) The banana leaves present the same color in both halves, which indicates that at both sides, the indicatrix makes the same angle with respect to the polarizers (black arrows). (b) When the central defect of the banana leaves makes an angle of  $45^\circ$  with respect to the polarizers both halves present extinction simultaneously. This fact indicates that the molecular directors make an angle of  $45^\circ$  with respect to the central defect at both sides. The width of the photographs is about  $600 \mu\text{m}$ .

texture change commented on above, it seems that an irreversible phase transition from a columnar ( $B_1$  type) to a smectic ( $\text{SmC}_A\text{P}_A$  type) phase occurs when a strong enough electric field is applied. This material can be added to the few examples of bent-core liquid crystals that exhibit similar field-induced phase transformations.<sup>20,21</sup>

A structural characterization of the C1 material was performed by means of small-angle X-ray measurements, which were carried out at various temperatures within the mesophase. Figure 5 represents the small-angle X-ray diagram obtained at  $156^\circ\text{C}$  on cooling. Two clear peaks (numbered 3 and 4 in Figure 5) whose positions differ in  $0.07^\circ$  are clearly distinguished, and a pair of small reflections (numbered 1 and 2) is also visible. A smaller peak appears at a larger Bragg angle (peak number 5). Although the number of independent reflections is similar to that usually expected for nonoriented liquid crystals samples, the possibility of performing an unambiguous indexing is limited, not only because the reflections are mainly concentrated within a narrow angular interval ( $\sim 0.4^\circ$ ) but also because

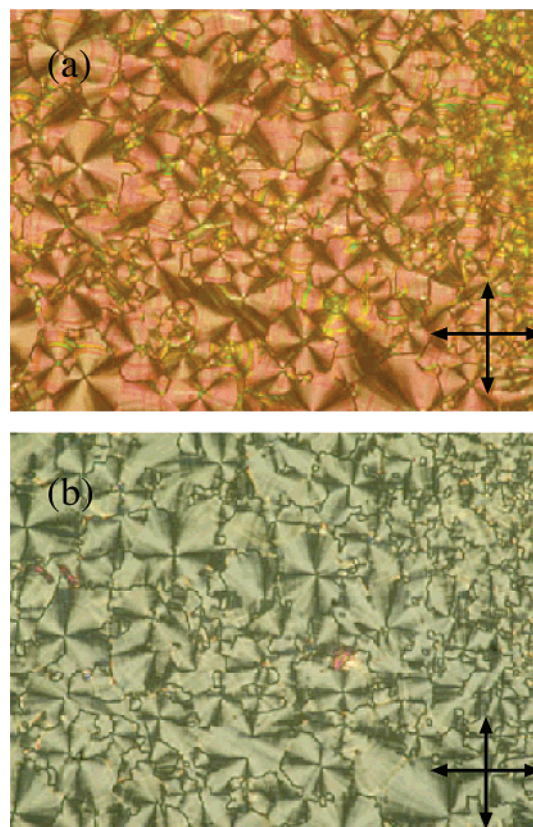


**Figure 4.** Photomicrographs of the textures of compound C1 in the SmCP phase induced by an electric field. (a) On cooling from the isotropic phase under a field of  $14 \text{ V}/\mu\text{m}$ , the material displays circular domains with the extinction brushes making an angle of about  $45^\circ$  with respect to the polarizers (black arrows). (b) Under no field the birefringence decreases, and the extinction brushes are parallel to the polarizers. This behavior is compatible with a  $\text{SmC}_A\text{P}_A$  ground state. The width of the photographs is about  $600 \mu\text{m}$ .

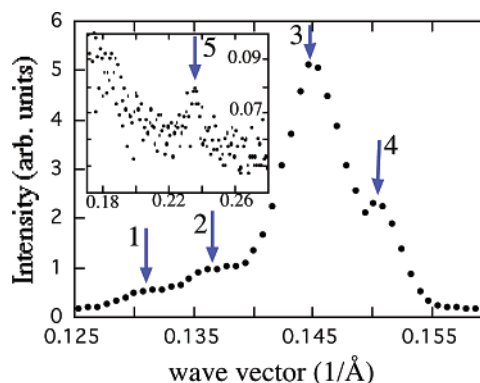


**Figure 5.** X-ray diffraction intensity as a function of the wave vector  $q = 4\pi/\lambda \sin \theta_B$ , where  $\lambda$  is the X-ray wavelength and  $\theta_B$  is the Bragg angle, for compound C1. Five peaks are observed for  $\theta_B < 2^\circ$ , which were indexed according to the following set of Miller indices: 1, (01); 2, (20); 3, (11); 4, ( $\bar{1}$ 1); and 5, (31).

two of them (peaks 1 and 2) are scarcely defined. In this respect, measurements performed on oriented samples, where the complete reciprocal lattice is obtained at once with a two-dimensional (2D) detector would permit a much more direct interpretation. A conclusion is, however, clear: the X-ray diagram of Figure 5 cannot be indexed on the basis of a rectangular lattice. This fact discards the possibility of a nontilted structure, which was one of the alternatives suggested from the optical analysis. Thus, the indexing of the diagram was carried out on the basis of an oblique 2D

(20) Ortega, J.; de la Fuente, M. R.; Etxebarria, J.; Folcia, C. L.; Diez, S.; Gallastegui, J. A.; Gimeno, N.; Ros, M. B.; Pérez-Jubindo, M. A. *Phys. Rev. E* **2004**, *69*, 011703.

(21) Amaranatha Reddy, R.; Sadashiva, B. K.; Raghunathan, V. A. *Chem. Mater.* **2004**, *16*, 4050.

lattice (see Figure 5). According to the selected indexing strategy, the intensity difference between the peak (11) and the peak  $(\bar{1}1)$  and the absence of a  $(\bar{3}1)$  reflection are in agreement with a synclitic structure (peaks of practically the same intensity for  $(hl)$  and  $(\bar{h}l)$  reflections would result for an anticlinic arrangement in a nearly rectangular lattice).<sup>11</sup> The resulting parameters are  $a = 92.0 \text{ \AA}$ ,  $c = 48.0 \text{ \AA}$ , and  $\beta = 87.5^\circ$ , and no appreciable variation of these parameters was detected within the temperature range of the mesophase. The  $c$  parameter, together with the molecular length ( $63.5 \text{ \AA}$ ), deduced theoretically by molecular modeling, assuming a bending angle of  $120^\circ$  and an all-trans conformation for the aliphatic chains, is compatible with a molecular tilt of about  $45^\circ$ . This means that the layer regions of the columnar structure are either perpendicular or parallel to the defect line of the banana leaves in Figure 3. Analogous conclusions were drawn by Takaniishi et al.<sup>22</sup> from the textures observed in liquid crystals composed by nontilted bent-shaped dimers.

Next, a structural model for the mesophase will be proposed through the analysis of the different electron density distributions that account for the observed X-ray diagram. This is one of the standard methods used in the crystallography of solids and was employed in the study of bilayer smectic liquid crystal phases<sup>23</sup> and also in three-dimensional liquid-crystal structures.<sup>24</sup> In our case, despite some possible controversy in the indexing of the X-ray diagram (with the consequent influence on the resulting structure), we consider it useful to extend this method to 2D liquid crystal phases. The method is as follows: a given  $hl$  reflection is due to the  $hl$  Fourier component of the periodic electron density  $\rho(x,z)$  of the structure. The amplitude and phase of this component are given by the complex structure factor  $F(hl)$ . Accordingly, we have

$$\rho(x,z) = \frac{1}{A} \sum_{hl} F(hl) \exp[-2\pi i(hx + lz)] \quad (1)$$

where  $x$  and  $z$  are in units of the lattice parameters  $a$  and  $c$  respectively, and  $A$  is the area of the unit cell.  $F(hl)$  is, in turn, related to the intensity of the  $hl$  reflection as  $I(hl) = |F(hl)|^2$ . Because  $\rho(x,z)$  is real,  $F(\bar{h}l) = F^*(hl)$ , and the following expression results:

$$\rho(x,z) = \frac{F(00)}{A} + \frac{1}{A} \sum_{hl} |F(hl)| \cos[2\pi(hx + lz) - \phi_{hl}] \quad (2)$$

where the  $h = 0, l = 0$  term was separated from the sum. This term is the average electron density of the unit cell, and  $\phi_{hl}$  are the phases of the structure factors  $F(hl)$ . In this equation we can see the nub of the problem of determining crystal structures: The amplitudes  $|F(hl)|$  are determined from the measured intensities, but the phases  $\phi_{hl}$  are not experimentally accessible. However, this essential difficulty may be in some cases worked out on the basis of the symmetry relations that the structure factor satisfies, together

with a suitable choice of the cell origin. For example, if  $\rho(x,z) = \rho(-x,-z)$  for a given origin of the unit cell, then the structure factor is real ( $\phi_{hl}$  is equal to 0 or  $\pi$ ) and, therefore,  $F(\bar{h}l) = F(hl)$ . This occurs when the layer group<sup>25</sup> of the system contains inversion centers or two-fold axes perpendicular to the lattice plane, as is the case of practically the whole set of structural models proposed up to now.<sup>4,9,26</sup> Thus, the problem of the phase reduces to the problem of the sign of  $F(hl)$ , and the electron density is expressed as

$$\rho(x,z) = \frac{F(00)}{A} + \frac{1}{A} \sum_{hl} \pm |F(hl)| \cos[2\pi(hx + lz)] \quad (3)$$

The correct sign combination is now decided by the physical merit of the obtained electron density map, with the aid of complementary knowledge of the system, such as packing conditions, molecular size, optimization of steric interactions, and so forth.

As shown in Figure 5, the reflections 3 and 4 are much more intense than the others. Consequently, every electron density distribution will depend almost exclusively on these reflections. On the other hand, the weak anomaly indexed as (01) in Figure 5 did not appear in some of the cooling or heating runs. Therefore, we assumed that this peak is not intrinsic to the high temperature mesophase. On the contrary, taking into account the field-induced transition to a lamellar phase in this material, it can be assumed that this anomaly is due to coexistence of a small volume of  $B_2$  phase in the bulk. The fact that the (01) peak can be incorporated to the indexing scheme of the 2D structure can be explained because the layer spacing of the field-induced phase calculated from the tilt deduced from Figure 4a and the molecular length is equal to the  $c$  parameter of the 2D structure. In view of this, we calculated  $\rho(x,z)$  from eq 3 considering only peaks 2, 3, 4, and 5. The symmetry of the electron density map is given, in principle, by the oblique plane group  $p2$ . This plane group imposes no relations between  $F(hl)$  and  $F(\bar{h}l)$  or  $F(hl)$ , as well as no systematic extinction rules for the indices  $h$  and  $l$ . However, we have chosen a nonstandard oblique basis for the X-ray diagram indexing, according to which (leaving aside the (01) anomaly) the  $(hl)$  reflections satisfy  $h + l = 2n$ , that is, the systematic extinction rule for a centered lattice. Therefore, in our case the symmetry of  $\rho(x,z)$  is given by the oblique planar group  $c2$ .

The relative integrated intensities of these peaks were obtained from the X-ray diagram after background subtraction and were corrected for the Lorentz and the polarization factors  $L$  and  $p$ , respectively, that correspond to our experimental geometry. Finally, to obtain the proper intensity  $I(hl) = |F(hl)|^2$  for the  $hl$  reflection, the intensity of each peak must be divided by its corresponding multiplicity, that is, the number of  $hl$  reflections with the same Bragg angle. In our case the multiplicity equals 2 ( $hl$  and  $\bar{h}l$ ) for all the peaks in Figure 5.

(22) Takaniishi, Y.; Izumi, T.; Watanabe, J.; Ishikawa, K.; Takezoe, H.; Iida, A. *J. Mater. Chem.* **1999**, *9*, 2771.

(23) Francescangeli, O.; Rinaldi, D.; Laus, M.; Galli, G.; Gallot, B. *J. Phys. II France* **1996**, *6*, 77.

(24) Zeng, X.; Ungar, G.; Imp  rator-Clerc, M. *Nat. Mater.* **2005**, *4*, 562.

(25) Kopsky, V.; Litvin, D. B., Eds. *International Tables for Crystallography, Subperiodic Groups*; Kluwer Academic Publishers: Norwell, MA, 2002; Vol. E.

(26) Tschierske, C.; Dantlgraber, G. *Pramana* **2003**, *61*, 455.

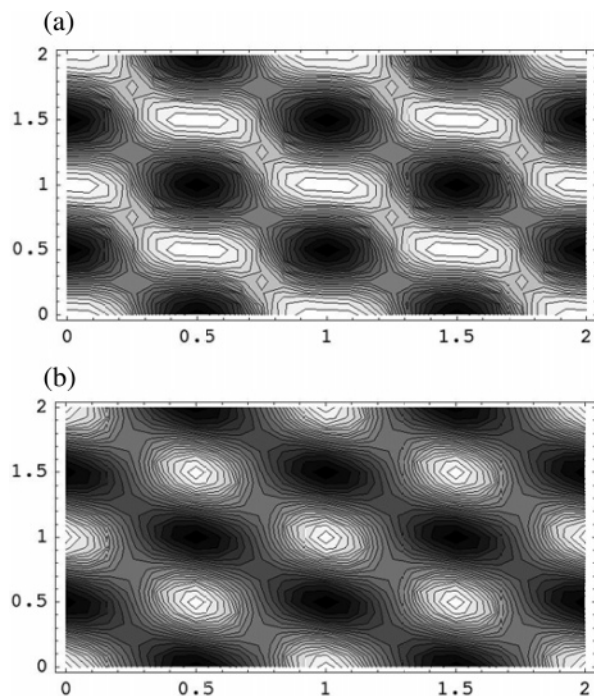


**Figure 6.** Electron density distributions of compound C1 calculated from expression 3. The brighter areas represent the regions of higher electron density. The signs for the (20), (11), (11), and (31) coefficients in eq 3 are chosen as  $(- + + -)$  for part a and  $(+ + + +)$  for part b. The values of  $|F(hl)|$  for the different  $(hl)$  Miller indices were obtained from the peak intensities of the X-ray diagram in Figure 5 (see text). The horizontal and vertical scales are in units of the lattice parameters  $a$  and  $c$ , respectively. The relation between  $a$  and  $c$  was taken as  $a/c = 2$ . The oblique  $\beta$  angle was approximated to  $90^\circ$  in both schemes.

Figure 6 represents the electron density distribution  $\rho(x,z)$  obtained from expression 3 for two different sets of signs for the (20), (11), ( $\bar{1}1$ ), and (31) terms. In particular this set was selected as  $(- + + -)$  for Figure 6a. The same pattern, except for a translation on the  $x,z$  plane, results for the sets  $(+ + - +)$ ,  $(+ - + -)$ , and  $(- - - +)$ . On the other hand, the map of Figure 6b corresponds to the sign combination  $(+ + + +)$ , although equivalent patterns are obtained for  $(- + - -)$ ,  $(- - + +)$ , and  $(+ - - -)$ . The set of the additional eight combinations obtained from those above, by means of a general inversion of signs, give similar electron density maps. A comment is in order regarding the (01) peak. Even when its exclusion was justified above, it was found that the consideration of this reflection in the calculation does not affect significantly the main features of  $\rho(x,z)$  apart from a very slight deviation from a centered structure. Summarizing, the patterns in Figure 6 represent the essential alternatives in electron density distributions that are compatible with the X-ray diagram. A difference is obvious between the maps in Figure 6. In Figure 6a the regions with higher electron density (white regions) tend to form stripes whose length is about half the cell parameter  $a$ . Furthermore, each stripe joins its adjacent stripes in such a way that almost continuous zigzags of high density parallel to the (11) lattice line are formed. On the other hand, in Figure 6b the highest electron density is practically concentrated in quite small regions.

Now, we consider the two possibilities represented in Figure 6 for the real structure. The bent-core molecules presumably pack in such a way that their central cores join together with their lateral structures parallel to each other.

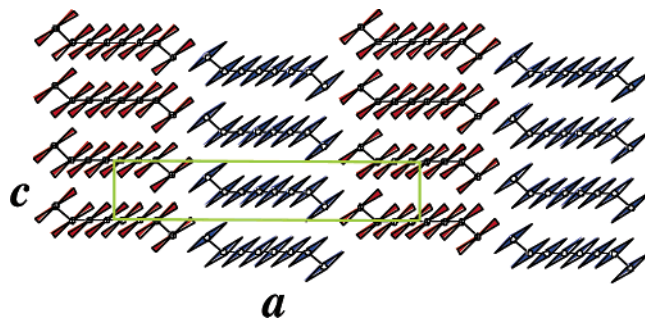


**Figure 7.** Structural model proposed for the  $Col_{ob}$  of compound C1. The molecular packing is in agreement with the electron density shown in Figure 6a. For simplicity, a rectangular cell ( $\beta = 90^\circ$ ) has been considered. The structure is synclinc and antiferroelectric, but the precise ordering of the chirality of the columns (indicated in red and blue colors) cannot be defined by standard X-ray measurements. With the combination of colors used in the figure the structure is a generalization of the  $B_{1rev}$  phase.

As a consequence of this, the cores tend to order themselves to form ribbons where the electron density is higher. It is evident that the pattern appearing in Figure 6b cannot support the existence of these ribbons and must be discarded. On the other hand, this packing model is clearly in agreement with the pattern of Figure 6a, where the molecular cores are distributed along the higher density stripes. A possible structure is shown in Figure 7, which is similar to the  $B_1$  reversed tilted phase, as was defined previously.<sup>27–29</sup> However, in our case the ribbons are bent at their extremes to permit suitable molecular packing in those regions and form a nearly rectangular lattice ( $\beta = 87.5^\circ$ ).

It is important to note that the structure represented in Figure 7 is only one of the possible structural models that are in agreement with our experimental results. This can be easily understood as follows: The diffraction diagram of a columnar 2D structure with lattice parameters  $a$  and  $c$  is reduced to the  $h0l$  reciprocal plane. Then, for nonresonant X-ray diffraction, the contribution to the structure factor of an atom with form factor  $f$  positioned at  $r = xa + yb + zc$  with respect to a given origin is  $f \exp[2\pi i(hx + lz)]$ ; that is, it does not depend on the  $y$  coordinate. This means that our diffraction experiment only detects a periodic distribution of bent-core molecules projected on the lattice plane. In other words, we cannot get information about the chirality of the ribbons, and any combination of the colors is possible in Figure 7. In our case, the compound C1 is not SHG active if no electric field is applied to the sample. This fact discards a ferroelectric arrangement of the columnar phase, and, therefore, red and blue ribbons must be present in equal number because the structure is synclinc. The precise order of the colors is, however, undefined.

## Results Obtained for the Material C2

On slow cooling from the isotropic phase the mesophase grows within the isotropic liquid as telephone-wire structures that are shown in Figure 8. On further cooling, the material

- (27) Szydłowska, J.; Mieczkowski, J.; Matraszek, J.; Bruce, D. W.; Gorecka, E.; Pocięcha, D.; Guillon, D. *Phys. Rev. E* **2003**, *67*, 031702.  
 (28) Mieczkowski, J.; Gomola, K.; Koseska, J.; Pocięcha, D.; Szydłowska, J.; Gorecka, E. *J. Mater. Chem.* **2003**, *13*, 2132.  
 (29) Pelz, K.; Weissflog, W.; Baumeister, U.; Diele, S. *Liq. Cryst.* **2003**, *30*, 1151.

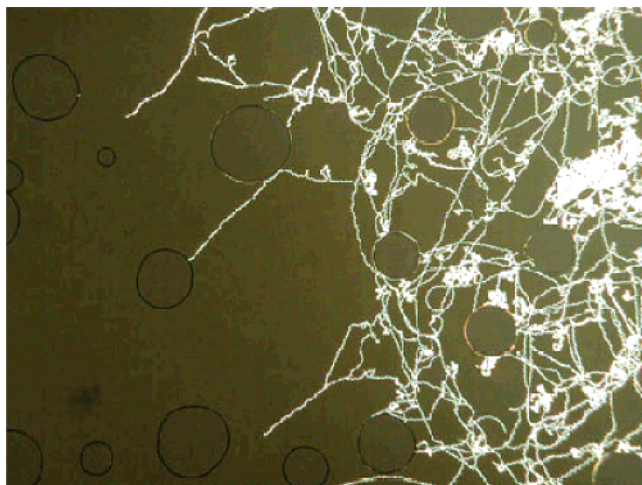


**Figure 8.** Telephone wires structures that the compound C2 exhibits when cooling from the isotropic phase. Photograph width about 600  $\mu\text{m}$ .



**Figure 9.** Fan-shaped texture of compound C2 under an electric field of 12 V/ $\mu\text{m}$ . The same extinctions are observed under field reversal, which indicates a racemic  $\text{SmC}_5\text{P}_A$  ground state. The width of the photograph is about 250  $\mu\text{m}$ .

enters completely the mesophase showing, under the polarization microscope, textures formed by small domains with fringes characteristic of the  $\text{SmC}_5\text{P}_A$  phase. In some regions of the sample, small circular domains appear with concentric fringes, being the brushes directed along the polarizer directions. Under an electric field of 12 V/ $\mu\text{m}$  the material presents ferroelectric switching. Under field the textures exhibit fan-shaped domains without fringes that remain unaltered under field reversal (see Figure 9). On the other hand, the birefringence of this phase with and without electric field was similar, about  $\Delta n = 0.04$ , which reinforces the hypothesis that the material presents a racemic structure.

In light of the above experimental evidences, it would be reasonable to assume the phase to present a  $\text{SmC}_A\text{P}_F$  structure under field and a  $\text{SmC}_5\text{P}_A$  structure in the absence of field. However, the growth of the mesophase in telephone-wire structures has been widely related to the existence of smectic undulated phases.<sup>8,9,30</sup> The X-ray diagram of these phases is characterized by strong commensurate reflections (indicating a layer structure) together with incommensurate satellites (as

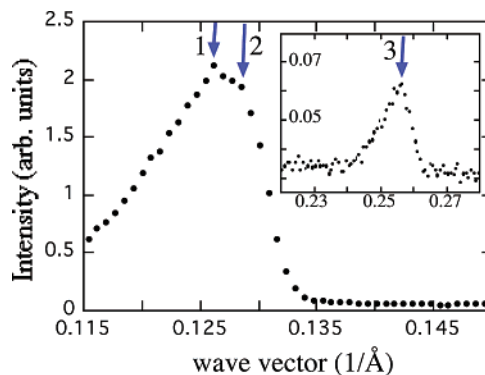


**Figure 10.** X-ray diffraction diagram for compound C2. Three peaks are observed for Bragg angles  $\theta_B < 2^\circ$ . The resulting Miller indices are 1, (01); 2, (11); and 3, (22).

a consequence of a one-dimensional undulation of the smectic layers).<sup>8,9,30</sup> Thus, to check the possibility of a similar structural model for material C2, small-angle X-ray diffraction experiments were carried out. The measurements were performed at different temperatures within the mesophase.

Figure 10 shows a typical intensity profile for Bragg angles  $\theta_B < 2^\circ$ , corresponding to the temperature  $T = 163^\circ\text{C}$ . The diagram shows only two clear peaks within this angular range, indicating, in principle, a normal smectic mesophase. However, if the shapes of both peaks are compared to each other, it seems that the highest peak may be considered a superposition of two reflections (1 and 2 in Figure 10), peak 3 being the second harmonic of peak 2. Peaks 2 and 3 show slight temperature dependence in such a way that the angular position of peak 3 is always double that of peak 2. On the contrary, peak 1 remains steady in the whole range of temperatures, and the periodicity distance associated to this reflection is compatible with the smectic spacing. Therefore, we consider a 2D orthogonal lattice as the simplest indexing scheme (see Figure 10) where the cell parameters obtained at 163  $^\circ\text{C}$  are  $a = 255.57 \text{ \AA}$  and  $c = 49.76 \text{ \AA}$ . The  $a$  parameter increases slightly as the temperature decreases, its values ranging between 255 and 263  $\text{ \AA}$  in the whole interval of measured temperatures.

In addition, it should be pointed out that assuming a molecular length of 63.5  $\text{ \AA}$ , in the most stable conformation of the core and an all-trans conformation for the aliphatic chains, the tilt angle obtained from the  $c$  parameter is  $38.5^\circ$ . This value of the tilt and the anticlinic molecular arrangement are in agreement with the small birefringence that the material exhibits. In fact, the birefringence value  $\Delta n = 0.04$  can be considered small for a material formed by molecules with azoxy linkages in their core.<sup>31</sup>

Following the strategy carried out with compound C1, the main features of the 2D structure can be obtained for C2. The X-ray diffraction diagram of compound C2 presents three peaks, the intensities of which are denoted as  $I_1$ ,  $I_2$ , and  $I_3$ . In this case, the rectangular symmetry of the electron density map imposes the following restrictions to the structure factor: On one hand,  $|F(hl)| = |F(\bar{h}l)|$ , that is, in our case the intensity of the (11) and ( $\bar{1}1$ ) reflections is the same. On the other hand, the existence of the (01) reflection

(30) Shreenivasa Murthy, H. N.; Sadashiva, B. K. *Liq. Cryst.* **2003**, *30*, 1051.

(31) Brunet-Germain, M. *Mol. Cryst. Liq. Cryst.* **1970**, *11*, 289.

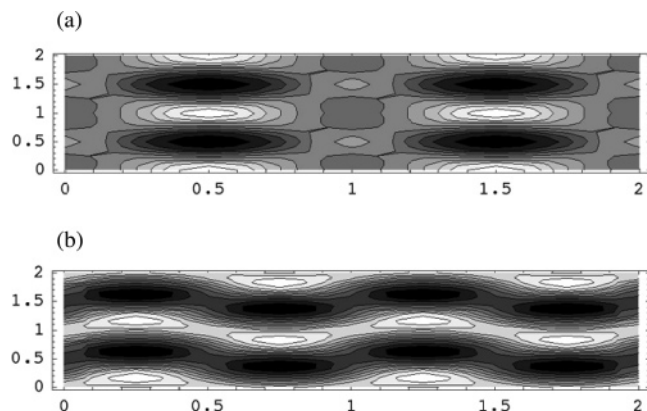


**Figure 11.** Electron density distributions of compound C2 calculated from expression 3. The brighter areas represent the regions of higher electron density. The signs for the (01), (1,1), (11), (22), and (22) terms in eq 3 are chosen as (+ - - +) for part a and (+ - + +) for part b (in both cases the fourth sign corresponds to that of the (22) and (22) coefficients). The values of  $|F(hl)|$  for the different (hl) Miller indices were obtained from the peak intensities of the X-ray diagram in Figure 10 (see text). The horizontal and vertical scales are in units of the lattice parameters  $a$  and  $c$ , respectively. The relation between  $a$  and  $c$  was taken as  $a/c = 5$ .

restricts the possible plane groups of the electron density map to  $pm2m$  and  $pm2g$ , in which case  $F(hl) = F(\bar{h}l)$  and  $F(hl) = (-1)^h F(\bar{h}l)$ , respectively. The main contribution to the electron density map is due to the double peak. Therefore, we will start neglecting the  $I_3$  contribution. As the structure is rectangular, the Fourier coefficients of the electron density must hold the following relations:

$$|F(01)| = \sqrt{I_1/2}, \quad |F(11)| = |F(\bar{1}1)| = \sqrt{I_2/4} \quad (4)$$

There are  $8 = 2^3$  different sets of sign combinations for those coefficients. However, four of them represent a phase shift of  $\pi$  in the whole set of Fourier coefficients of the electron density function and will be considered later. The four remaining sign combinations can be taken as (+ - +), (- - +), (+ - -), and (- - -). It can be shown that the first and second possibilities lead to the same electron density structure and are related by a shift in the coordinate origin. The same situation occurs between the third and fourth sign sets. Therefore, only two independent density maps must be considered, that is, (+ - +) and (+ - -).

If now we include the contribution of  $I_3$ , the choice of the sign for the coefficients  $F(22)$  and  $F(\bar{2}2)$  only duplicates the number of density structures considered above because  $F(22) = F(\bar{2}2)$ . On the other hand, the maps with different signs only for that coefficient do not represent changes qualitatively significant in the structural models, given the small size of the peak 3. Figure 11a,b is representative of the density maps for the two main possibilities and correspond to the sign sets (+ - - +) and (+ - + +), respectively (the fourth sign corresponds to the  $F(22)$  coefficient). In this figure, one can also appreciate that the electron densities corresponding to a general sign inversion of the Fourier coefficients do not give rise to qualitatively new structures. Thus, we do not need to consider additional possibilities for the sign sets.

Regarding now the two alternatives of Figure 11, the one presented in Figure 11a must be discarded because it would imply the existence of stripes of low electron density along the lattice vector  $c$ , which energetically represents a very

unfavorable packing of the molecules. On the contrary, Figure 11b shows an electron density that basically represents a smectic undulated structure, the modulation of which seems to be close to a sinusoidal one. In that sense, it resembles the structure proposed by Coleman et al.<sup>9</sup> for the  $B_7$  phase of the banana-shaped compound named MHOBOW in ref 9. However, some differences between both structures can be pointed out. On one hand, in Figure 11b it can be clearly seen that the contour lines of the electron density inside the layer are not parallel to the smectic layers everywhere. In fact, there are regions along the layer in which the contour lines are almost perpendicular. This means that the structure is not a perfect undulated smectic but that the electron density is slightly modulated inside the layers. In addition, even if this electron density modulation is neglected, the smectic layer undulation cannot be assumed to be simply sinusoidal. In fact, in the case of a perfect sinusoidal undulation, the intensity of the different X-ray diffraction peaks for a given index value  $l$  must hold the following relation:<sup>32</sup>

$$\frac{I(h_1 l)}{I(h_2 l)} = \frac{J_{h_1}^2(2\pi \frac{l}{c} B)}{J_{h_2}^2(2\pi \frac{l}{c} B)} \quad (5)$$

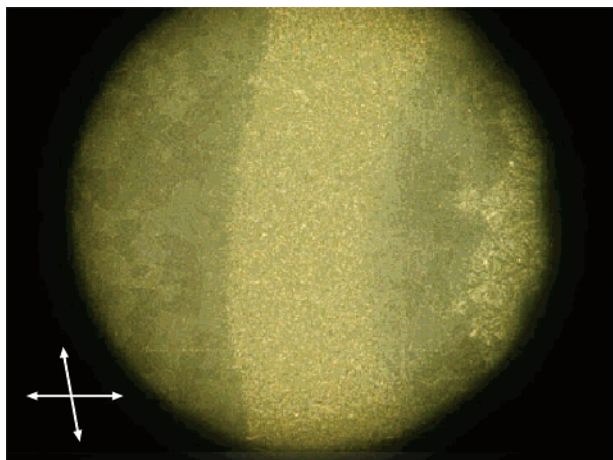
where  $J_{h_i}$  is the  $h_i$ th Bessel function of the first kind,  $h_1$  and  $h_2$  are the indices associated to the reciprocal vector  $a^*$  of two different peaks, and  $B$  is the amplitude of the sinusoidal modulation of the smectic layer. From Figure 11b it could be assumed for a perfect sinusoidal undulation an amplitude value  $B \approx c/3$ , and, therefore, the ratio of intensities for, for instance, peaks (01) and (11) should be according to eq 5  $I(01)/I(11) = 0.088$ . Therefore, taking into account the multiplicities of both reflections,  $I_1/I_2 = 0.044$ . However, in Figure 10 both peaks are similar. This result supposes a clear disagreement with the assumption of a simply sinusoidal undulation.

A final comment could be raised regarding the phase structure of this compound after having applied an electric field. With our experimental equipment, it has not been possible to clarify if the material undergoes an irreversible phase transition to a  $SmC_5P_A$  phase after field application, or on the contrary, its ground state always presents undulated smectic layers. The clarification of this point would require X-ray diffraction experiments under an electric field, which is beyond the limits of our experimental facilities.

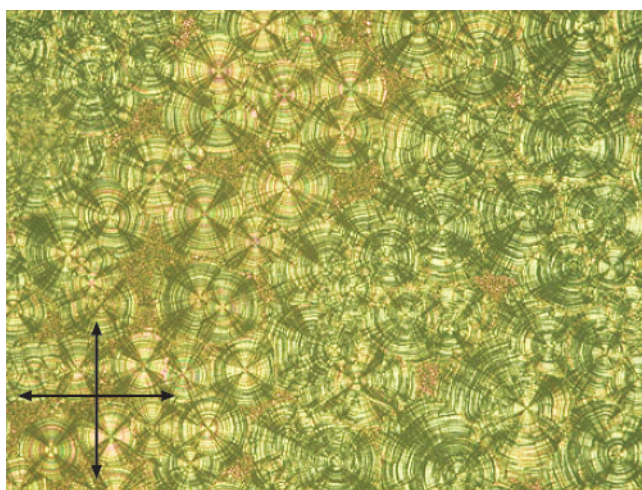
### Results Obtained for the Material C3

Figure 12 shows the optical textures in the mesophase of compound C3 on cooling from the isotropic liquid. There is a thermal gradient in the photographs from left to right. Three regions with two types of textures can be appreciated, one at the middle of the photographs and the second one at the left and right extremes. The different textures were obtained using different cooling rates, fast-slow-fast on going from left to right. In other words, small-grain chirality domains

(32) Folcia, C. L.; Ortega, J.; Etxebarria, J. Presented at the 20th International Liquid Crystal Conference, Ljubljana, Slovenia, 2004; Poster STR-P076.



**Figure 12.** Textures of the  $\text{SmC}_A\text{P}_A$  phase exhibited by compound C3. In the figure, three different regions can be appreciated that correspond to different cooling rates from the isotropic phase (fast–slow–fast starting from the left). On fast cooling (extreme parts) the textures present no birefringence, and gyrotropic domains can be observed under slightly uncrossed polarizers (white arrows). Photograph width about  $3000 \mu\text{m}$ .



**Figure 13.** Optical textures in the  $B_2$  ( $\text{SmCP}$ ) phase of compound C3 on cooling from the isotropic phase under an electric field of  $8 \text{ V}/\mu\text{m}$ . The structure is  $\text{SmC}_S\text{P}_F$  with a tilt angle close to  $45^\circ$ . Black arrows indicate the polarizer directions. The width of the photograph is about  $600 \mu\text{m}$ .

are formed for rapid cooling whereas the more conventional  $B_2$  textures result for slow cooling. The  $B_2$  ( $\text{SmCP}$ ) assignment is confirmed by X-ray measurements. Only two sharp peaks are detected at small angles, which correspond to the first and second orders of a given periodicity, and a diffuse peak is found at wide angles. The smectic spacing deduced from the X-ray diagram is  $42.0 \text{ \AA}$ , which corresponds to a tilt  $\theta = 48^\circ$  for a theoretical molecular length of  $63.5 \text{ \AA}$ .

Figure 13 shows the texture obtained at a low cooling rate and under a direct current (dc) field. As can be seen, the extinction directions are approximately at  $45^\circ$  from the polarizers directions. This is consistent with the tilt value deduced from the X-ray data. The phase should correspond to a  $\text{SmC}_S\text{P}_F$  structure under field. Without field the structure is  $\text{SmC}_A\text{P}_A$ .

It is interesting to comment on the textures obtained on rapid cooling. Two regions almost isotropic but with opposite optical rotations are observed. Similar textures with even smaller grain size have been previously observed and also interpreted successfully as due to a  $\text{SmC}_A\text{P}_A$  structure.<sup>33</sup> To

observe the optical rotation, the birefringence should be very small. This is accomplished in the present case for two reasons. First, a tilt angle close to  $45^\circ$  in an anticlinic structure gives rise to a small birefringence. Second, there is an averaging effect of the (already small) birefringence because of the random domain distribution and small domain size in the rapidly cooled samples. In contrast, the gyrotropy does not average to zero, but a gyration effect remains. The effective gyrotropy is equal to one-third of the trace of the gyrotropic tensor of one domain.<sup>33</sup> Estimates of the gyrotropy of a  $B_2$  phase are in agreement with the order of magnitude of the observed rotation ( $1^\circ/\text{mm}$ ).<sup>33,34</sup>

### SHG Measurements

Detailed SHG measurements were carried out on the mesophase of compound C1 under field ( $\text{SmC}_S\text{P}_F$ ) because it has two azo groups, so its efficiency was expected to be one of the highest of the three studied materials. The contracted susceptibility of the  $\mathbf{d}$  tensor, which describes the SHG process in the homochiral states, can be approximated as follows:<sup>6,35</sup>

$$d_{ij} = \begin{pmatrix} 0 & 0 & 0 & D \sin \theta \cos \theta & D \cos^2 \theta & 0 \\ 0 & 0 & 0 & D \sin^2 \theta & D \sin \theta \cos \theta & 0 \\ D \cos^2 \theta & D \sin^2 \theta & d & 0 & 0 & D \sin \theta \cos \theta \end{pmatrix} \quad (6)$$

where  $\theta$  is the tilt angle,  $D = Nf^2\beta_{\xi\xi\xi\xi}$ , and  $d = Nf^2\beta_{\xi\xi\xi\xi}$ . Here,  $N$  is the density of molecules and  $f$  is a local field factor.  $\beta_{\xi\xi\xi\xi}$  and  $\beta_{\xi\xi\xi\xi}$  are the hyperpolarizability components referenced to the coordinate frame of Figure 2. The tensor is referenced to a  $(xyz)$  frame in which  $x$  is perpendicular to the smectic layers and  $z$  is parallel to the polar axis. According to a previous work,<sup>7b</sup> the material is aligned homeotropically in the cell gap on applying an electric field parallel to the cell glasses.

In this situation the  $\mathbf{d}$  tensor can be obtained by means of SHG measurements at normal incidence. Two different input–output configurations were used: p–p, with both the polarizer and the analyzer parallel to the polar axis, and s–p, with the first polarizer rotated  $90^\circ$ . At both sides of the gap there was an unaligned region in the sample which responded to the field but had no effect on the SHG signal, a point verified later by covering the edges of the gap with aluminum sheets.

Neglecting the absorption at  $532 \text{ nm}$  (we measured an optical density of 0.17 for a thickness of  $5 \mu\text{m}$  at the isotropic phase), the SHG power  $P^{2\omega}$  is given by

$$P^{2\omega} \propto d_{\text{eff}}^2 \frac{\sin^2\left(\frac{2\pi\delta nL}{\lambda}\right)}{\left(\frac{2\pi\delta nL}{\lambda}\right)^2} \quad (7)$$

(33) Ortega, J.; Folcia, C. L.; Etxebarria, J.; Gimeno N.; Ros, M. B. *Phys. Rev. E* **2003**, *68*, 011707.

(34) Hough, L. E.; Clark, N. A. *Phys. Rev. Lett.* **2005**, *95*, 107802.

(35) Ortega, J.; Pereda, N.; Folcia, C. L.; Etxebarria, J.; Ros, M. B. *Phys. Rev. E* **2001**, *63*, 011702.

where  $d_{\text{eff}} = d$  for the p-p and  $d_{\text{eff}} = D \sin^2 \theta$  for the s-p configurations, respectively;  $\delta n = n^{2\omega} - n^\omega$  is the difference of refractive indices between the second harmonic and the fundamental waves for that configuration;  $\lambda$  is the fundamental wavelength; and  $L$  is the sample thickness. The constant of proportionality is determined after the calibration of the setup using a y-cut quartz plate ( $d_{11} = 0.4 \text{ pm/V}$ ). The Fresnel transmission coefficients were also incorporated into the calculations.

We used the same method as that in ref 7, employing cells of different thicknesses. In this way, we first found out the values of  $\delta n$  for each configuration and then determined the parameters  $D$  and  $d$ . The final results, together with the estimated errors, were the following:

$$\delta n^{s-p} = n_z^{2\omega} - n_y^\omega = 0.027 \pm 0.003$$

$$\delta n^{p-p} = n_z^{2\omega} - n_z^\omega = 0.035 \pm 0.003$$

$$d = 3.3 \pm 0.2 \text{ pm/V}$$

$$D = 6.1 \pm 0.7 \text{ pm/V}$$

The magnitude of the SHG susceptibility is similar to that found in the classical family of banana-shaped compounds named P-n-O-PIMB in ref 7a. This behavior is logical because in that family the charge-transfer process at the lateral cores due to the imine group is expected to be similar to that of the compound containing the azo group.

### Photoinduced Effects

As a final point we discuss briefly the photoactivity of the materials. Planar samples were illuminated with polarized laser light. We employed an Ar<sup>+</sup> laser emitting at 488 and 515 nm and a He-Cd laser emitting at 442 nm. The average intensity of irradiation on the samples was about 100 mW/cm<sup>2</sup>. Similar effects were observed in the three materials for the three wavelengths. The studies were carried out under a dc electric field, and the textures were simultaneously observed in the polarizing microscope.

Upon illumination within the mesophase an initial decrease of the birefringence takes place and, after a few seconds, the samples undergo an isothermal transition to the isotropic phase. As soon as the light is removed, the illuminated zone

enters back into the mesophase forming unaligned small domains. This behavior agrees with the results reported in the literature.<sup>16-18</sup> The effect is interpreted as a consequence of the trans-cis photoisomerization of the -N=N- bond: under suitable light irradiation, the cis population increases, so the molecules lose their original bent shape, and the material becomes isotropic. Once the light is off, the cis population diminishes as the -N=N- linkages return to the more stable trans configuration. The cis-trans conversion takes place in short times (less than 1 s) in these relatively high temperatures, where thermal isomerization is important.

### Conclusions

Three bent-core mesogens possessing photoactive linkages have been studied. The structures of the different mesophases have been analyzed, finding columnar and smectic phases. The structural models have been deduced from the analysis of the electron density distributions, using data both from the positions (Bragg angles) and intensities of the X-ray diffraction peaks. This approach contrasts with that used in standard X-ray studies, where the reflection intensities are seldom used to get any structural information.

Regarding the nonlinear optical properties, we have shown that the azo moieties maintain the SHG efficiency and the resulting **d** tensor is similar to that found in imine-derivative compounds; thus, both groups lead to high mobility of the electron density. Finally, and as a last point, we would like to remark that the presence of the azo- or azoxybenzene structures adds a new dimension to these materials because it permits photocontrol to be gained in some of their physical properties.

**Acknowledgment.** I.A. and I.P. thank the Ministry of Education of Spain and the Aragón Government (DGA), respectively, for grants. This work was supported by the CICYT-FEDER of Spain-EU (Project No. MAT2003-07806-C02), the University of the Basque Country (Project No. 9/UPV 00060.310-13562/2001), and the Aragón Government.

**Supporting Information Available:** Detailed experimental section and characterization data (PDF). This material is available free of charge via the Internet at <http://pubs.acs.org>.

CM060256P